Electronic Supplementary Material (ESI) for CrystEngComm.

Supporting Information

Intermetallic Pd_3Pb square nanoplates as highly efficient electrocatalysts for oxygen reduction reaction

Sai Luo, Min Tang, Xingqiao Wu, Yang Ou, Zeyi Wang, Ni Jian, Xiao Li, Yangfan Lin, Yucong Yan, Jingbo Huang, Hui Zhang,* Deren Yang

State Key Laboratory of Silicon Materials & School of Materials Science and Engineering, Zhejiang University, Hangzhou, Zhejiang 310027, P. R. China.

*Correspondence to: msezhanghui@zju.edu.cn

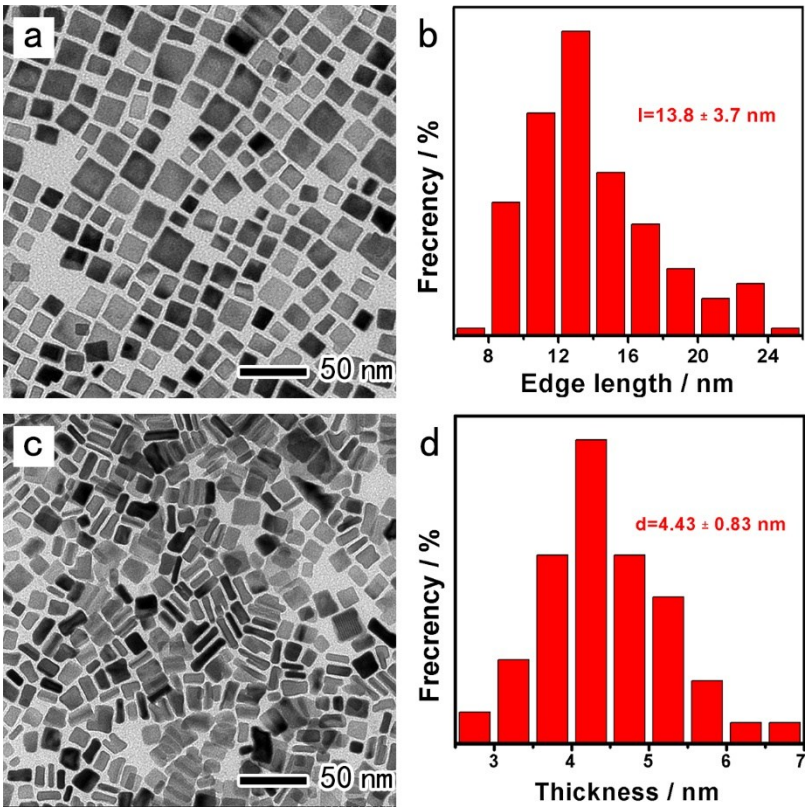

Figure S1. (a, c) Representative TEM images at low magnification, (b) edge length distribution and (d) thickness distribution of the Pd_3Pb square nanoplates prepared using the standard procedure.

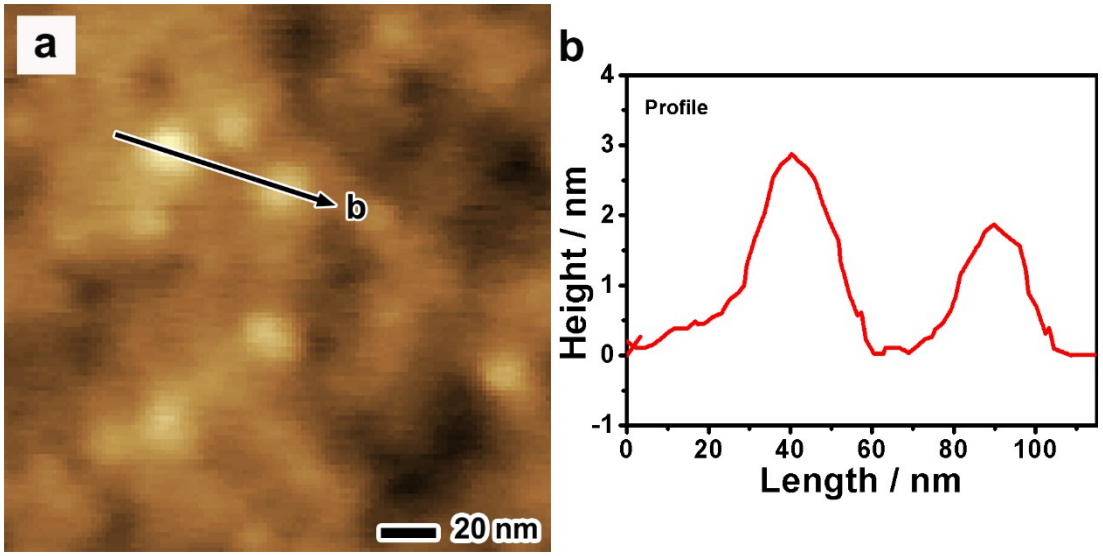

Figure S2. (a) AFM image and (b) corresponding height profile of Pd_3Pb nanoplates.

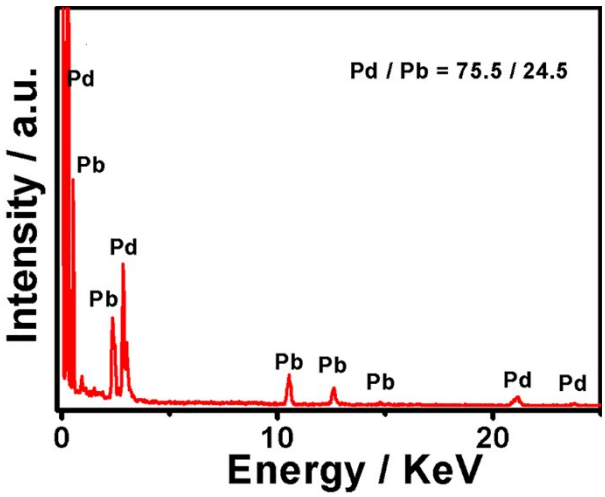

Figure S3. EDX spectrum of the intermetallic Pd_3Pb square nanoplates, showing a Pd/Pb atomic ratio of 3.08:1.

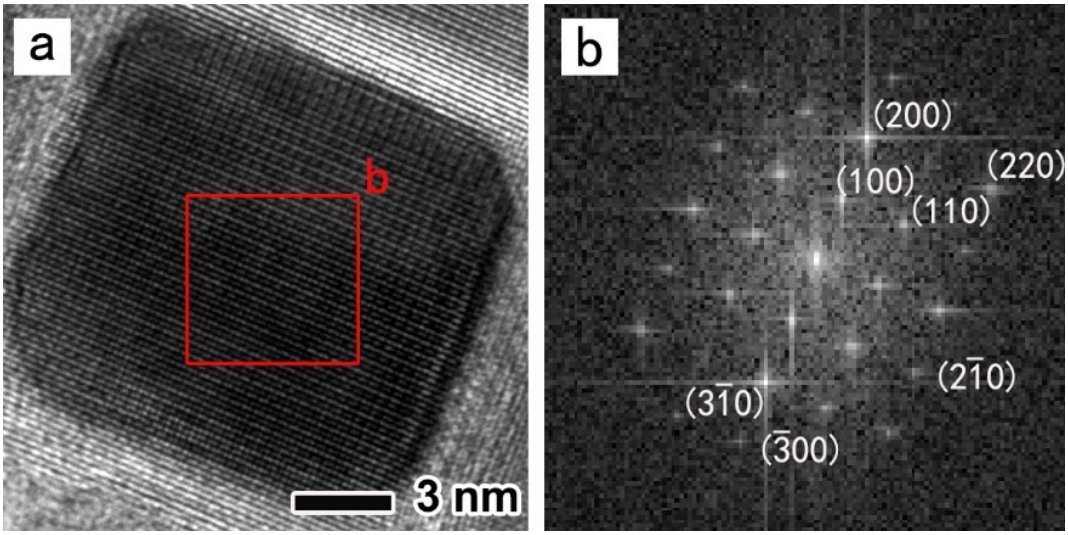

Figure S4. (a) High-resolution TEM image of a single Pd_3Pb square nanoplate. (b) FFT pattern arising from high-resolution TEM image of the part marked by the red rectangle in (a).

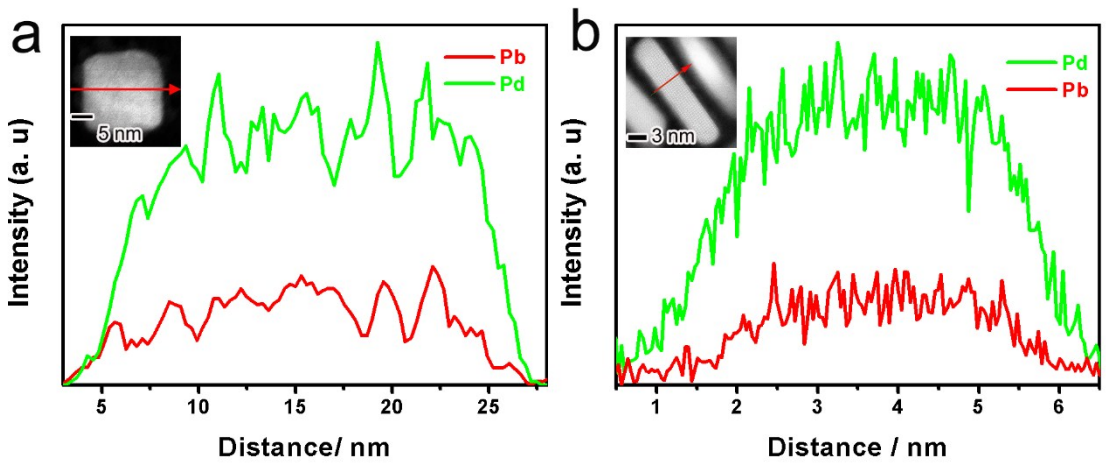

Figure S5. EDX line-scan profiles of (a) a planar Pd_3Pb nanoplate and (b) a vertically upstanding Pd_3Pb nanoplate. The insets show the corresponding HADDF-STEM images.

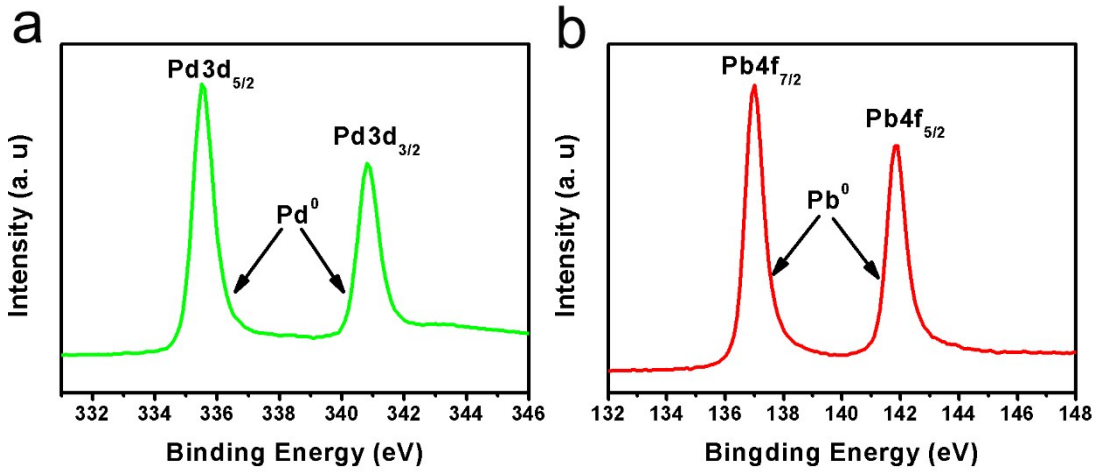

Figure S6. XPS spectra of the Pd_3Pb intermetallic nanoplates for (a) Pd 3d and (b) Pb 4f orbitals, respectively.

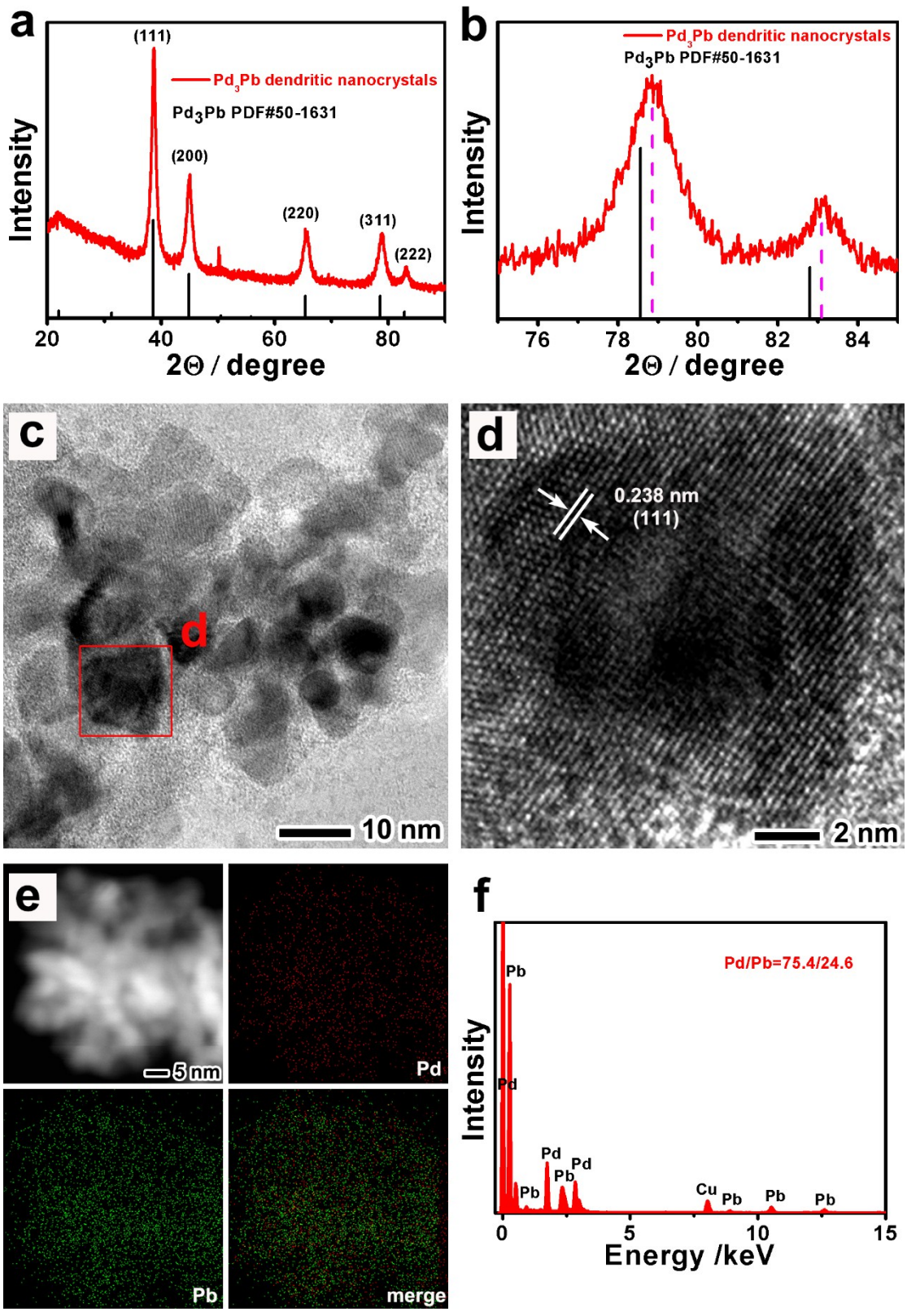

Figure S7. (a, b) XRD pattern and its corresponding magnified one, (c, d) HRTEM images, (e) EDX-mapping and (f) EDX spectrum of the Pd_3Pb alloy dendritic nanocrystals.

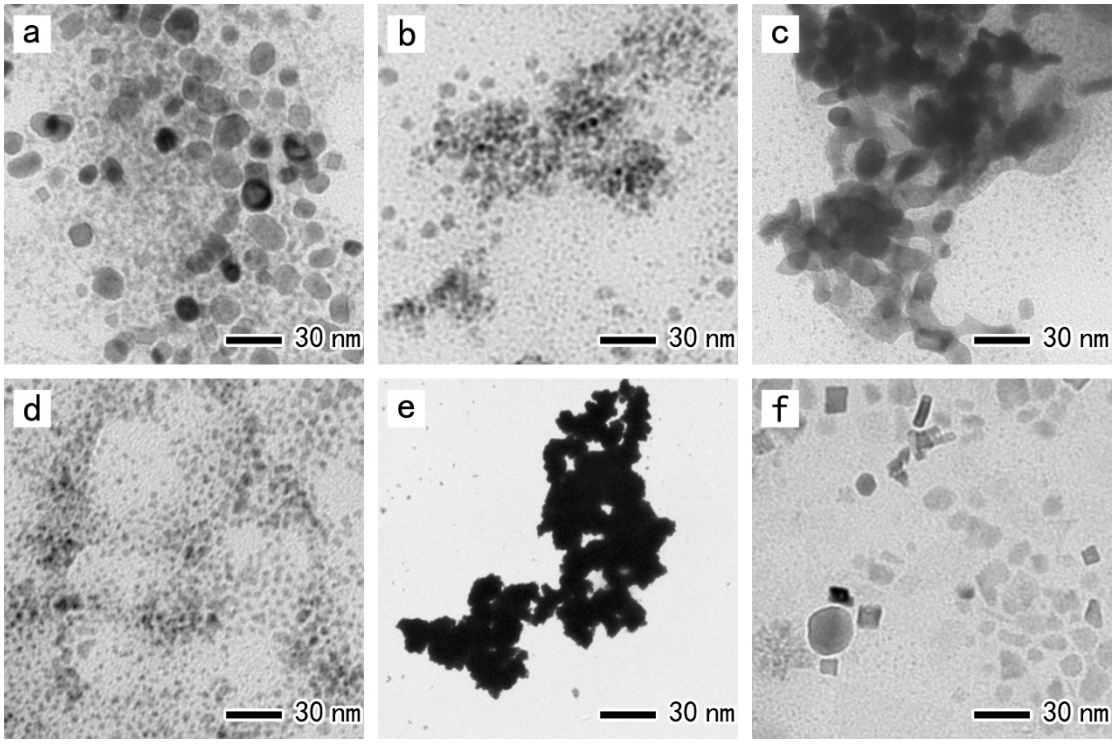

Figure S8. Representative TEM images of the products prepared by using the starndard procedure except for different molar ratios of Pd to Pb precursors: (a) in the absence of Pb precursor, (b) 2:1, (c) 1:1, (d) 1:2, (e) 1:3 and (f) in the absence of Pd precursor.

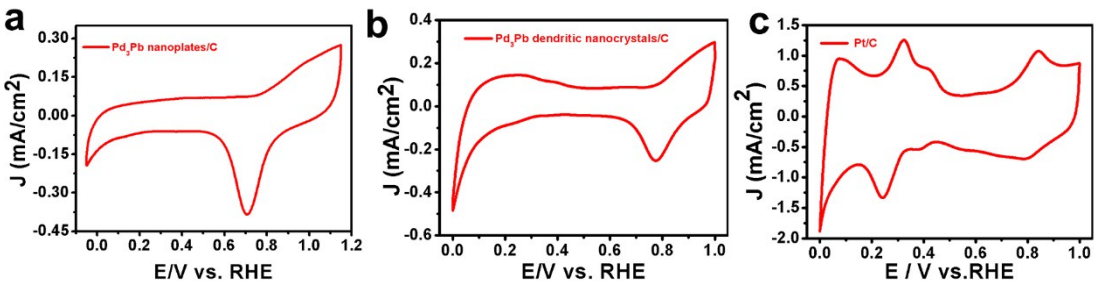

Figure S9. The cyclic voltammetry (CV) curves of (a) the Pd_3Pb square nanoplates, (b) Pd_3Pb dendritic nanocrystals, (c) commercial Pt/C in Ar-purged 0.1 M KOH solutions at a sweep rate of 50 mV/s.

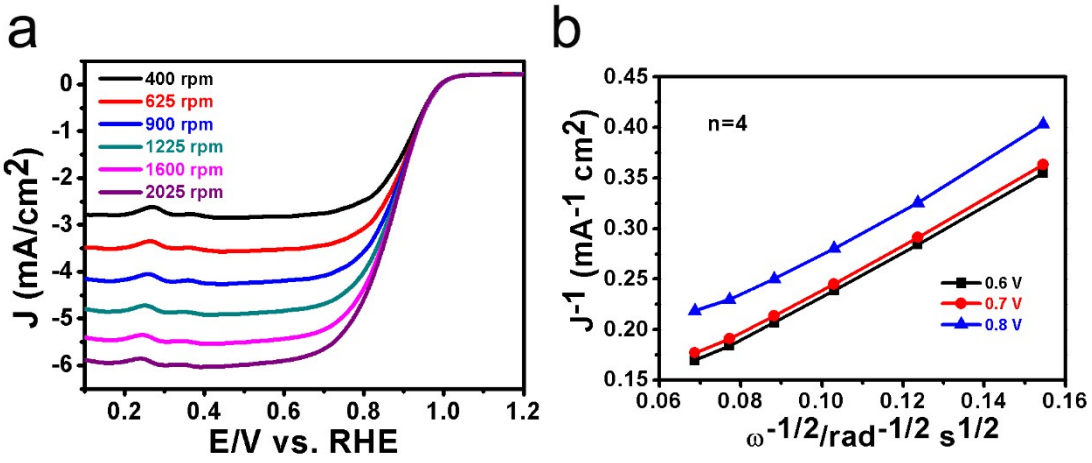

Figure S10. (a) Rotating-disk voltammograms of Pt/C in O_2-saturated 0.1 M KOH at different rotation rates with a sweep rate of 10 mV s^{-1}. (a) The corresponding Koutechy-Levich plots of figure (a).

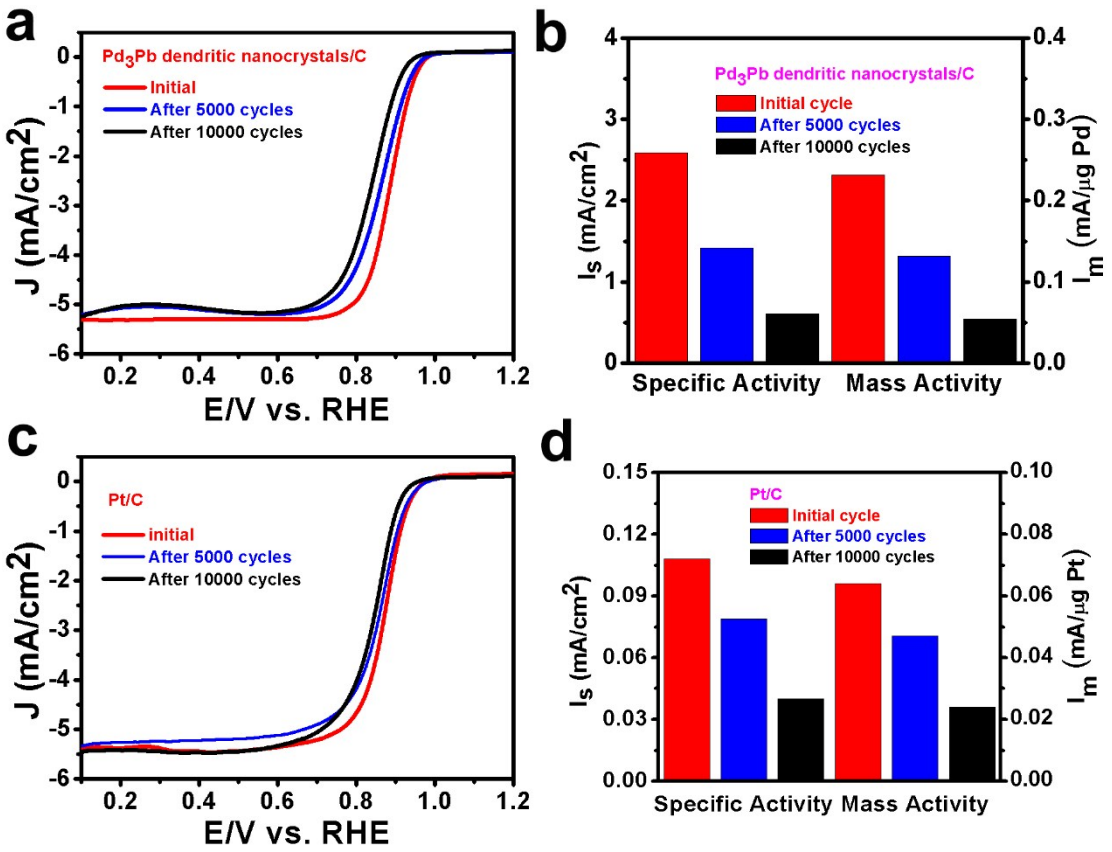

Figure S11. (a, c) ORR polarization curves of Pd_3Pb alloy dendritic nanocrystals/C and Pt/C in O_2-saturated 0.1 M KOH before and after different potential cycles between 0.6 and 1.0 V versus RHE, respectively. (b, d) The changes on specific and mass activities of the Pd_3Pb alloy dendritic nanocrystals/C and Pt/C after various potential cycles between 0.6 and 1.0 V versus RHE, respectively.

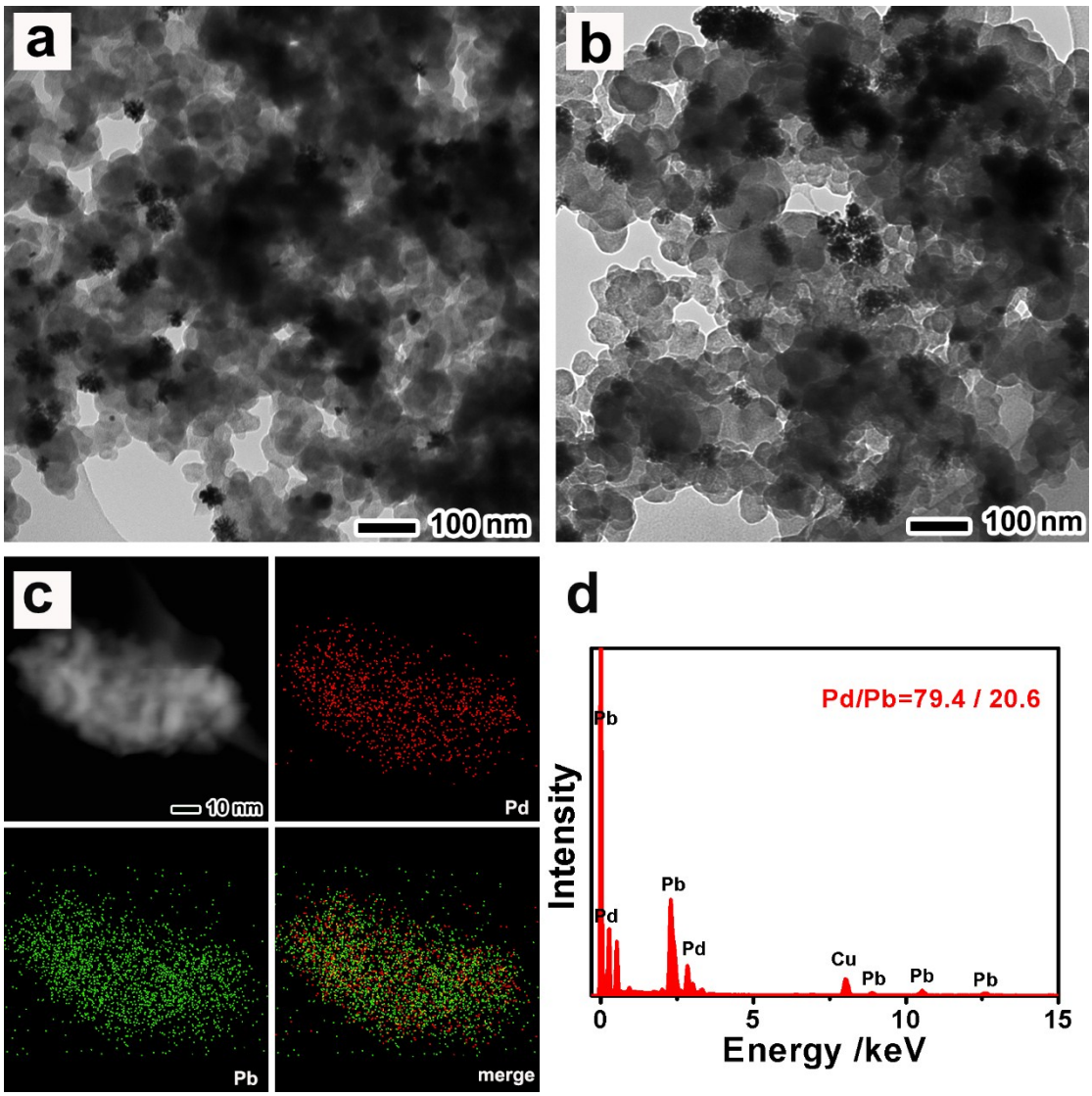

Figure S12. Representative TEM images of the Pd_3Pb alloy dendritic nanocrtstals/C (a) before and (b) after ADT. (c) HADDF-STEM-EDX mapping image and (d) EDX spectrum of the Pd_3Pb alloy dendritic nanocrtstals after 10000 cycles between 0.6 V and 1.0 V versus RHE.

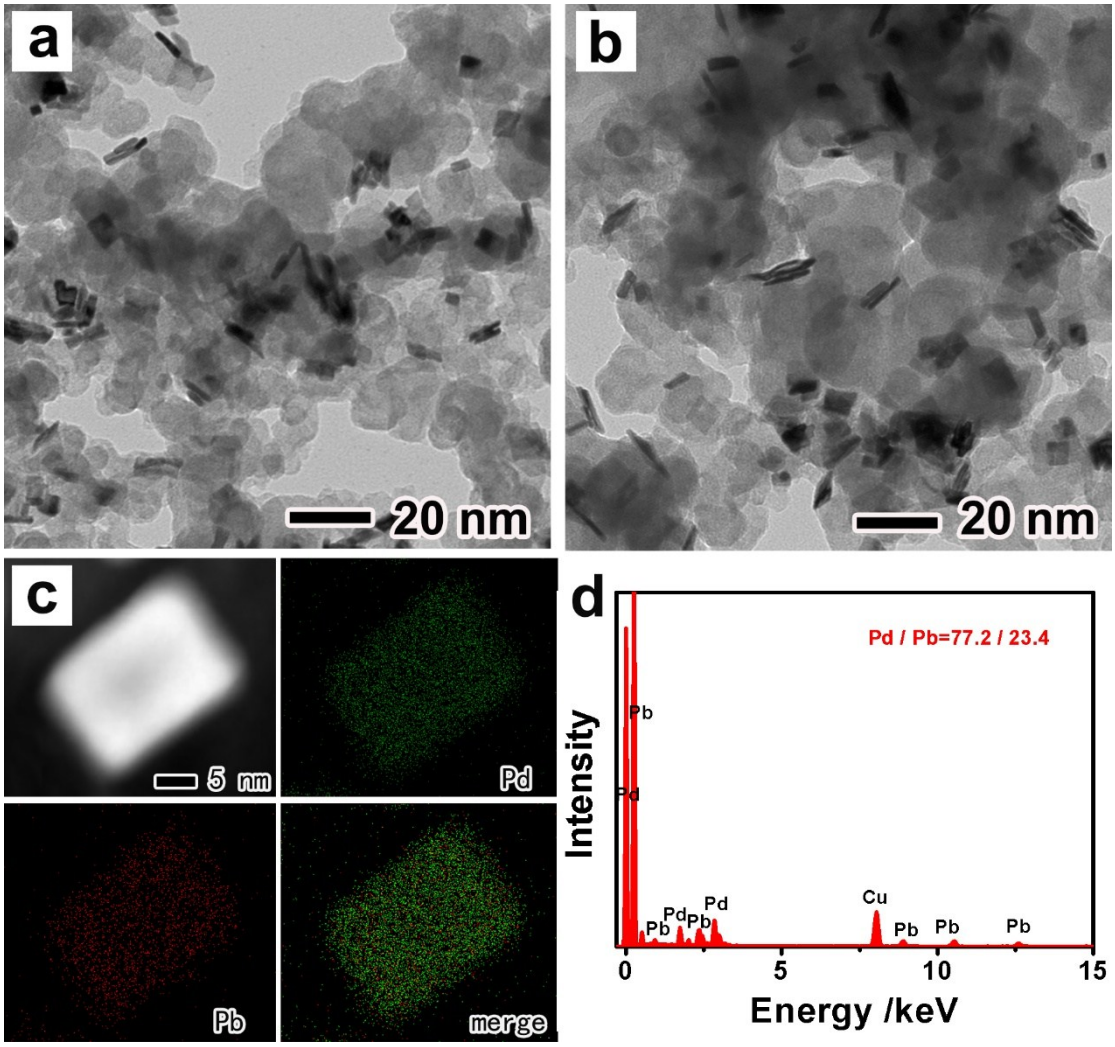

Figure S13. Representative TEM images of the intermetallic Pd_3Pb square nanoplates/C (a) before and (b) after ADT. (c) HADDF-STEM-EDX mapping image and (d) EDX spectrum of the intermetallic Pd_3Pb square nanoplates after 10000 cycles between 0.6 V and 1.0 V versus RHE.

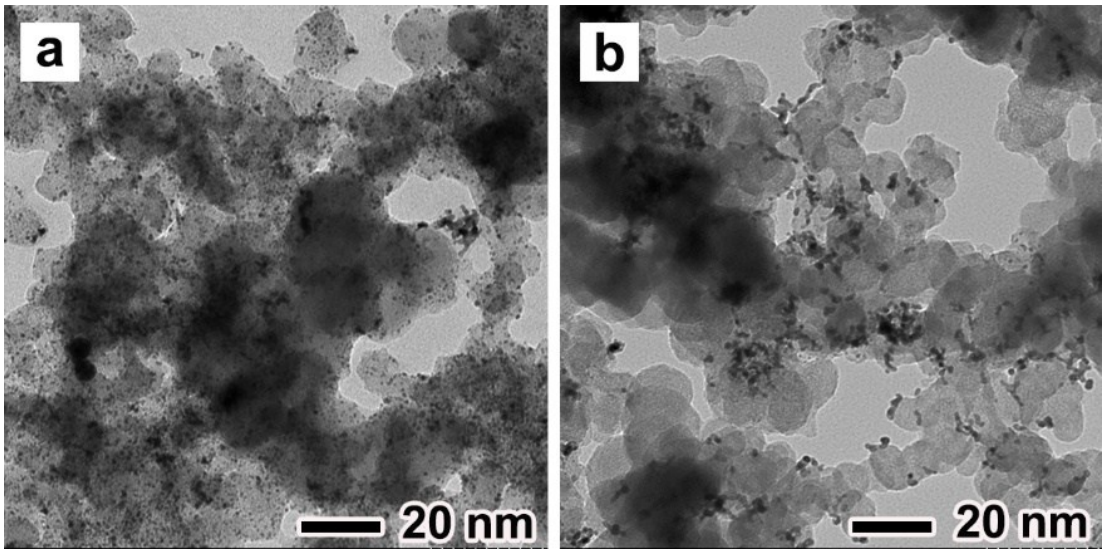

Figure S14. Representative TEM images of the commercial Pt/C (a) before and (b) after 10000 potential cycles between 0.6 V and 1.0 V versus RHE.